CHALMERS
UNIVERSITY OF TECHNOLOGY

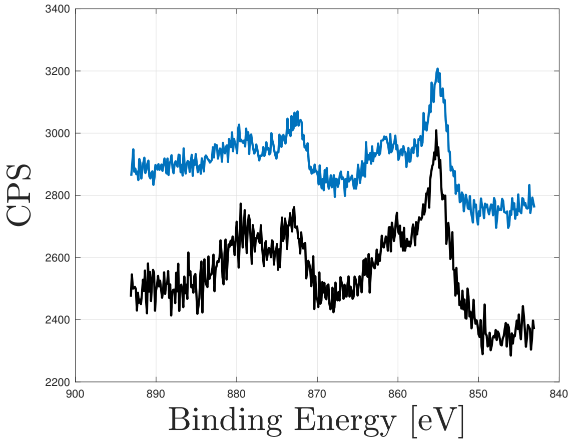

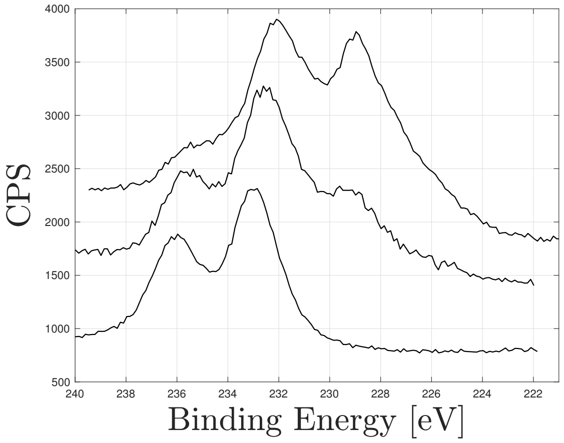

Reduced NiMo catalysts for hydrodeoxygenation of lignin model compounds

AMANDA SJÖGREN

Department of Chemistry and Chemical Engineering
CHALMERS UNIVERSITY OF TECHNOLOGY
Gothenburg, Sweden 2019

Bachelor's thesis 2019

Reduced NiMo catalysts for hydrodeoxygenation of lignin model compounds

AMANDA SJÖGREN

Department of Chemistry and Chemical Engineering
Division of Chemical Engineering
Chalmers University of Technology
Gothenburg, Sweden 2019

Reduced NiMo catalysts for hydrodeoxygenation of lignin model compounds
AMANDA SJÖGREN

Supervisor: Muhammad Abdus Salam, Chemistry and Chemical engineering
Examiner: Derek Creaser, Chemistry and Chemical Engineering

Bachelor's Thesis 2019
Department of Chemistry and Chemical engineering
Division of Chemical Engineering
Chalmers University of Technology
SE-412 96 Gothenburg
Telephone +46 31 772 1000

Reduced NiMo catalysts for hydrodeoxygenation of lignin model compounds

AMANDA SJÖGREN
Department of Chemistry and Chemical engineering
Chalmers University of Technology

Abstract

In this thesis work, the activity and product selectivity of reduced NiMo/γ-Al_2O_3 and NiMo/Yzeolite were compared with sulfided catalysts. Also, an unpromoted reduced Mo/Yzeolite catalyst was compared with a promoted reduced NiMo/Yzeolite catalyst. A model compound with a typical lignin linkage was used for all experiments. The experiments with the reduced catalysts were conducted within this project, whereas experimental results from sulfided catalysts were provided by the collaborating research group. Temperature programmed reduction (TPR) of calcined NiMo catalysts was carried out to gain insight about the reduction temperatures. After the reduction of the catalysts in the activation step, X-ray photoelectron spectroscopy (XPS) was conducted to study the oxidation states of the metals on the catalyst. The TPR showed that the NiMo/γ-Al_2O_3 should have been reduced in the catalyst activation step. On the contrary, the TPR result for the NiMo/Yzeolite did not confirm this. However, results from XPS showed that all catalysts had been partly reduced. Both sulfided NiMo/γ-Al_2O_3 and NiMo/Yzeolite catalysts showed greater HDO activity than the corresponding reduced catalysts. In the comparison of unpromoted and promoted catalysts, the result indicated that the promoted catalyst had higher HDO activity.

Acknowledgements

I would like to thank Derek Creaser and Louise Olsson for the chance to perform my thesis work in their research group. Furthermore, many thanks to Muhammad Abdus Salam, my supervisor, who helped me out with the experiments.

Amanda Sjögren, Gothenburg, January 2019

Contents

1. Introduction

Historically, biomass has played a key role as a source of energy for humans, but with the discovery of fossil fuels it lost its role as the main energy source [1]. Fossil fuels are non-renewable resources and they are one of the main causes of climate change due to their high yield of carbon dioxide when they are combusted. Compared to fossil fuels, fuels derived from biomass are considered renewable sources of energy since the carbon dioxide released from the combustion is restored in plants via the carbon cycle [2]. Both the environmental impact and the energy needs for today, and in the future, make the need for clean and sustainable fuels substantial. Therefore, a major challenge today is to replace fossil fuels with sustainable alternatives [3]. Research is being dedicated to the improvement of the production of biofuels and a necessary step in the production of them is the removal of oxygen in order to achieve bio-based hydrocarbons of higher quality and stability similar to fossil fuels [4, 5]. In addition to oxygen, other impurities such as sulfur and nitrogen need to be removed in refinery processes. This is carried out with a catalyst under a hydrogen pressure and is called hydrotreating [6]. Hydrodeoxygenation (HDO) is a type of hydrotreating process where the removal of oxygen is the key objective. In comparison to fossil components, biomass feedstocks also have many functional groups and are therefore a potential source of different chemicals aside from biofuels. However, it is a challange to find ways to produce chemicals with desired functionality [7].

The major parts of plant materials are cellulose, hemicellulose and lignin where lignin contributes to about 30 wt% of the material [8]. Lignin is a low-value side-products in some industrial processes and today, the vast majority of it is burnt to produce heat and power and only a small part is used for commercial applications [9]. Since biomass consists of a great amount of lignin, the valorization of it would make biorefineries a competitive alternative for petroleum refineries.

When lignin has been fractioned out from the biomass, the first step in converting lignin into value-added products is depolymerization followed by upgrading of the derived compounds [8, 9]. Depolymerization of lignin can be done in different ways. For example, pyrolysis, gasification and liquefaction [9]. A pyrolysis process is carried out in the absence of oxygen and depending on the reaction temperatures, the type of catalyst as well as the structure of the lignin itself, different linkages will break. Gasification is partial oxidation of lignin which produces syngas, a mixture of H_2, CO, CO_2 and CH_4 [10]. For pyrolysis and gasification to be efficient, the biomass must not consist of too much moisture. If so, liquefaction is a better option because the reaction is carried out in a solvent [7].

In lignin, 40-60 % of the linkages are β-O-4 ether bonds [11] and thus, breakage of this bond is often the objective of depolymerization of lignin [3]. Furthermore, lignin is a complex organic polymer with cross-linkages where the type of monomers vary among different species. To understand the chemistry of the depolymerized lignin and due to the complexity of lignin, model compounds with specific linkages are used. The reactivity and product selectivity of these compounds give information about lignin itself [9, 12]. The main objective for studies regarding lignin valorization is to understand different catalytic reactions where aromatic compounds are produced. This means that the catalyst must be selective for ether bond cleavages and not convert the aromatic rings during processes [11].

In hydrotreatment of bio-oils, sulfided NiMo catalysts are proven to be efficient [4]. However, to keep the catalyst in a sulfided and active form additional sulfur is needed during the process [3]. Another way to activate NiMo catalysts is by reduction [5]. It is therefore of interest to study the catalytic reactions of a model compound with a β-O-4 ether linkages using reduced NiMo catalysts.

1.1. Aim

The aim of this thesis project is to study the activity and product selectivity of reduced NiMo catalysts.

1.2. Delimitations

The model compound 2-phenethyl phenyl ether (PPE) (Figure 1), with a typical β-O-4 linkage, will be used. Also, two different support materials, γ-Al_2O_3 (γ-alumina) and ultra-stable Y zeolite, will be used. The γ-alumina is purchased from Sasol (Puralox SCCa 150/200) and the particle size is 60-150 μm [13]. The collaborating research group have previously determined the BET surface area, pore volume and average pore size to 199 gm^{-2}, 0.48 cm^3g^{-1} and 97.6 Å respectively [14]. The Yzeolite is purchased from Zeolyst International (CBV720). The SiO_2/Al_2O_3 mole ratio, the unit cell size and the surface area are 30, 24.28 Å and 780 gm^{-2} respectively [15].

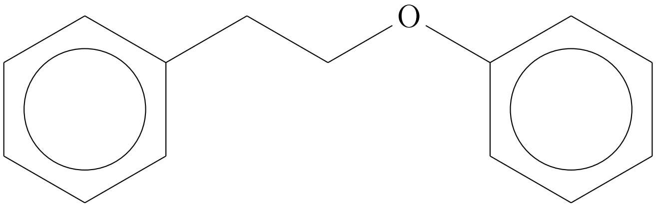

Figure 1: 2-phenethyl phenyl ether.

2. Theory

2.1. Catalysts

A catalyst increases the rate of a chemical reaction by enabling an alternative reaction pathway. Different catalysts can promote different pathways and consequently, the product selectivity can be different between catalysts. In homogeneous catalysis, the catalysts as well as the reactants and products are in the same phase whereas heterogeneous catalysts are in s separate phase, most often solids. In the latter case, the reaction is taking place on the surface of the solids [16]. HDO catalysts are usually heterogeneous [5].

In addition to the catalyst, promotors can be used to increase the rate of a reaction and improve selectivity or stability [17, 18]. For NiMo catalysts, molybdenum (Mo) is considered the active metal and nickel (Ni) is the promotor where Ni's role for sulfided NiMo catalysts is to enable adsorption for oxygenated compounds by facilitating creation of vacancies on MoS_2. The vacancies act as sites were oxygen-containing compounds can adsorb and these are the active sites of the catalyst [14]. The reduction of the metal oxides in a calcined NiMo catalyst creates oxygen vacancies which may act as the active sites for reduced NiMo catalysts [19].

Catalysts can also be supported by various materials to increase the surface area and in addition, the activity. Also, the support materials make the catalysts more stable by both maintaining the metallic dispersion during a process and giving mechanical strength resulting in better resistance to high temperatures and changes in pressure [20]. For HDO catalysts, the most commercially used support material is γ-Al_2O_3. Zeolite is another support that has been used successfully in conversion of residual bio-oils into different products [5]. One type of zeolite, which is commonly used in the cracking of crude oil, is the ultra-stable Y zeolite [21].

2.2. Gas Chromatography

Gas chromatography (GC) enables separation of components, usually called analytes, in a sample. The analytes are vaporized before they are introduced into the column and transported through it by a carrier gas. The time at which an analyte will reach the end of the column depends on its interaction with a stationary phase, which is either a nonvolatile liquid or a solid.

A mass spectrometer (MS) can be connected to the GC to enable a qualitative analysis of the sample. In MS, the analytes will be ionized and separated on their mass to charge ratio and identification of individual analytes are done based on the mass spectra. A common detector for quantification of carbohydrates is the Flame ionization detector (FID) where the electric signal from the electrons produced in the flame is proportional to the number of carbons in the destructed analyte [22].

2.3. Temperature Programmed Reduction

Transition metal oxides can occur in several stable oxidation states. When the synthesis of NiMo catalysts are finished, the metals are present in varying stable oxide forms [5]. In temperature programmed reduction (TPR), the rate of the reduction of the active component in a sample is measured while the temperature changes according to a pre-programmed schedule. The component is reduced by a reducing agent, in gas phase, of known concentration. Usually, the reducing agent is H_2 in argon (Ar). The following reaction will take place when H_2 is the reducing agent,

$$M_xO_y(s) + H_2(g) \rightarrow M(s) + H_2O, \tag{1}$$

where changes in the concentration of H_2 will be detected by some type of detector and information about the reduction potential at certain temperatures is obtained [23].

2.4. X-ray Photoelectron Spectroscopy

For heterogeneous catalysts, the reaction occurs on the surface and to assemble information about the surface layer of a catalyst, x-ray photoelectron spectroscopy (XPS) is a suitable method since it returns information about the first layers of a sample. An x-ray photoelectron beam will irradiate the sample and the principle behind the technique is measuring kinetic energies of emitted photoelectrons. The difference between the kinetic energy of the emitted electron and the energy of the monochromatic X-ray source gives information about the binding energy of the electron shells [24]. This enables insight about the different oxidation states of a metal. A difficulty with this method, however, is the interference of energy levels [20].

2.5. BET Theory

The specific surface area of a catalyst can be determined by the Brunauer – Emmett – Teller (BET) method. The theory of the BET method is a multilayer adsorption theory where the amount of the adsorbed and desorbed gas is measured as a function of gas pressure [25]. The BET equation is given by

$$V_{tot} = \frac{V_{mono} c p}{(p_0 - p)[1 + (c-1)\frac{p}{p_0}]} \tag{2}$$

where V_{mono} is the volume of the monolayer on the solid surface, V_{tot} is the total volume adsorbed at a given pressure, p is the vapor pressure of the gas, p_0 is the saturation vapor pressure and c is a constant which is related to the adsorbed gas. A linear form of Equation 2 is

$$\frac{p}{V_{tot}(p_0 - p)} = \frac{1}{V_{mono} c} + \frac{(c-1)p}{V_{mono} c p_0}. \tag{3}$$

An isotherm plot of Equation 3 gives a straight line at some initial relative pressure, typically $0.06 < \mathrm{P/P}^\circ < 0.3$. The monolayer V_{mono} can be determined from this region of the plot. The surface area, S_{BET} (volume/mass unit), is calculated from

$$S_{BET} = \frac{V_{mono} N_A A}{M} \times 10^{-20} \tag{4}$$

where N_A is Avogardo's number, A is the projected area of one adsorbate molecule on the surface and M is the molar volume.

In addition to information about the surface area, the pore volume as well as the pore size can be determined from physisorption experiments. A gas will condensate into a liquid below its saturation point and the partial pressure at which this takes place can be related to the pore size [26]. The Kelvin equation,

$$ln\Big(\frac{P}{P^\circ}\Big) = -\frac{2\gamma V_m}{RTr}, \tag{5}$$

relates the relative pressure and the size of a spherical pore. Here, γ is the surface tension, V_m is the molar volume of the liquid gas phase, T is the temperature, R is the gas constant and r is the radius of the sphere [25]. In most cases, for values of

P/P° > 0.4 a hysteresis behavior is observed and depending on the pore structure, the appearance can be more or less complicated. This means that Equation 5, which is only valid for spherical pores, is a generalization since the pores can have more complex structures. The hysterisis behavior is a consequence of condensation in pores occurring more easily than evaporation [24]. Barrett, Joyner, and Halend have developed a theory (BJH theory) on how to calculate the pore size and the pore volume by modifying the Kelvin equation [25, 24].

3. Methods

The plan for this thesis work was to run experiments with NiMo/γ-alumina and NiMo/Yzeolite catalysts. Additionally, a third catalyst was used, unpromoted Mo/Yzeolite to compare its selectivity and activity with the NiMo/Yzeolite.

3.1. Catalyst Synthesis

The catalysts containing Ni and Mo on pre-calcined γ-alumina and ultra stable zeolite Y as the support materials were already prepared by the team via wet impregnation process. Metal precursors used were ammonium molybdate tetrahydrate and nickel (II) nitrate hexahydrate for the impregnation of 15 wt% Mo and 5 wt% Ni respectively. The resulting catalysts, after drying, were calcined at 450 °C for 2 hours.

3.2. Catalyst Activation

In the catalyst activation step, approximately 0.6 g of catalyst was used. To activate the catalysts, they were reduced by hydrogen at a temperature of 450 °C in a 300 mL Parr autoclave reactor for 4 hours. 450 °C is the upper limit for this specific reactor. Due to the temperature, a graphite gasket (Flex Graph 2-1/2"ID) was used to seal the reactor, with 35 foot pounds torque needed to fully seal it. To remove oxygen from the reactor, approximately 5 bar nitrogen was flushed through it three times and to remove the nitrogen, the same pressure of hydrogen was flushed through it three times. To make sure that there was no gas leaking from the reactor, it was pressurized to 10 bar of hydrogen and after 15 minutes the pressure was compared with the initial one. If the pressure remained the same and the portable hydrogen detector gave no indication of hydrogen leakage from the reactor, the temperature was increased to start reduction of the catalyst. After the reduction, some of the reduced catalyst was recovered in a small vial and ethanol was added to prevent the catalyst from oxidizing in the presence of air. Later, the recovered catalyst was analyzed by XPS to investigate the oxidation states of the surface metals.

3.3. Catalytic Activity Test

The activity tests were also carried out in a 300 mL Parr autoclave reactor. First, 0.55 g of the catalyst was added to the reactor and 125 mL of n-dodecane was as added as quickly as possible to prevent the catalyst from being exposed to air, which may cause oxidation. Then, 5.8 g of 2-phenethyl phenyl ether was added, which represents 5 mol% of the total feed. When all chemicals were added, a teflon gasket (Virgin PFTE 2-1/2"ID) was placed on the reactor and to seal the reactor a torque of 32 foot pounds was used. Nitrogen was used to flush the reactor to make sure no oxygen was present during the experiments. The reactor was filled with 5 bar of nitrogen and then emptied. This was repeated three times and the same procedure was carried out with hydrogen to remove the nitrogen. After flushing with both nitrogen and hydrogen, the reactor was pressurized to 10 bar of hydrogen. The portable hydrogen detector was used to make sure that the reactor was well tightened. Before starting the experiment, the reactor was heated up to 320 °C and a low stirring rate of 40-50 rpm was used in this step. When the temperature reached 320 °C, both the stirring rate and hydrogen pressure was increased to 1000 rpm and 50 bar respectively. This time was considered as the start of the experiment. Liquid samples were collected at 35, 60, 120, 180, 240, 300 and 360 min intervals. First, the stirring was turned off for the catalyst to settle in the reaction mixture. Second, a 1-2 mL sample was collected and discarded to make sure a more representative sample was collected. Then, a 1-2 mL sample was collected and hydrogen was added to the reactor to compensate for the pressure drop and the stirring was turned on again to 1000 rpm. In the end of each experiment, the catalyst was collected and kept for further possible characterization.

3.4. Sample Analysis

The collected liquid samples were centrifuged at 1500 rpm for 2 min for the catalyst to settle. Then, 200 µL of each sample was transferred to a small vial for GC analysis (Aglient 7890-5977A). The column that was used is a non-polar HP-5 capillary column with the dimensions: 30 m of length, 0.25 mm in diameter and a film thickness of 0.25 µm. The injector temperature was 325 °C. Initially, the oven temperature was kept at 100 °C for one minute. Then, it was heated at a rate of

10 °C/min until it reached 190 °C. After that, it was heated to 300 °C at 30 °C/min and kept at 300 °C for 1.3 min. For identification and quantification, MS and FID detectors were used respectively. The temperature for the FID detector was 335 °C. The software that was used for data analyses was MassHunter data analysis with the NIST library. External calibration curves for 2-phenethyl phenyl ether, ethylbenzene and phenol were measured for quantification of the analytes.

3.5. Catalyst Characterization

3.5.1. Temperature programmed reduction

The optimal reduction conditions for the NiMo catalysts were established using TPR. The unpromoted Mo catalyst was not tested because the TPR was carried out before the decision to use unpromoted catalyst was taken. For TPR, SENSYS differential scanning calorimetry (DSC) followed by MS (Hiden Analytical HPR 20 quadrupole MS) were used. For the analysis, approximately 10 mg of the catalyst was put into a quartz tube with sintered bed and then placed in the SENSYS calorimeter. Hydrogen was used as the reducing agent at a concentration of 2000 ppm in argon and with a flow rate of 20 mL/min. Before the hydrogen was introduced, pure argon was used and the temperature was kept at 300 °C for one hour to remove impurities and then cooled down at a rate of 20 ° C/min. When the hydrogen was introduced the temperature was increased at a rate of 10 ° C/min until it reached 800 ° C. The temperature was kept at a constant value of 800 °C for two hours and then it was cooled down at a rate of 50 ° C/min.

3.5.2. X-ray Photoelectron Spectroscopy

For XPS, a Perkin Elmer PHI 5000C ESCA system was used. Carbon rubber pads were placed on sample holders and the catalysts were placed on top of the carbon surfaces. A pipette was used to transfer the catalysts that were kept in ethanol. When the ethanol had evaporated from the sample droplets, the sample holder was placed in the pre-treatment sample chamber using a manipulator fork. The transfer to the main chamber was carried out when the sample chamber had reached an acceptable pressure of $2{\cdot}10^{-8}$ torr or less. The X-ray source was a monochromatic Al Kα with a binding energy of 1486.6 eV and the angle between the source and the detected electrons was 90°. A low energy electron gun was used to neutralize the sample and minimize the charging effects. The C1s peak with a binding energy of 284.6 eV was used as a reference.

3.5.3. Physisorption test

To determine the surface area, the pore volume and the pore size of the catalysts, the BET and BJH theory was used in a physisorption test. The apparatus for this was a Micrometrics ASAP 2010 instrument and liquid nitrogen was used for the physisorption analyses. Approximately 0.2 g of calcined catalyst was put into a round bottom flask and then degassed at 250 °C for 3 hours before the physisorption test was conducted at a temperature of 77 K. For the physisorption test, the relative pressure of nitrogen was measured as a function of adsorption and desorption.

4. Results and Discussion

The plan for this project was to use two different catalysts, NiMo catalysts with γ-Al_2O_3 and ultra stable zeolite Y as support materials. After a discussion about the role of nickel for sulfided catalysts, it was decided that an experiment with an unpromoted Mo/Yzeolite should be conducted to compare with the NiMo/Yzeolite in the case of reduced catalysts. At this time, TPR had already been conducted. Additionally, XPS results of calcined catalysts were provided by the collaborating group which had not analyzed the calcined Mo/Yzeolite. Therefore, TPR and XPS analyses of calcined Mo/Yzeolite are not presented in this report. BET took place when the decision to use the Mo/Yzeolite was taken and all three catalysts were tested in the physisorption experiment.

4.1. Catalyst Characterization

Calcined NiMo/γ-alumina and calcined NiMo/Yzeolite catalysts were examined using TPR. Results from the two experiments can be seen in Figure 2. These show that the temperature needed to start reduction of NiMo/γ-alumina is approximately 300 °C and for NiMo/Yzeolite it is approximately 500 °C. For the activation of the catalysts, the maximum temperature of 450 °C was used. According to the TPR result of NiMo/γ-alumina, 450 °C is high enough for reduction to start and the catalyst had likely been at least partly reduced. For the NiMo/Yzeolite, however, the TPR result give no clear indication that the catalyst should have been reduced in the catalyst activation step.

A notable difference between NiMo/γ-alumina and NiMo/Yzeolite is the hydrogen consumption characteristics. For NiMo/γ-alumina, several small peaks appear, which could be due to one metal being reduced in steps or due to different metals being reduced. A previous study of TPR of NiMo/γ-alumina suggests that at 400-500 °C, the reduction of Mo^{6+} to Mo^{4+} occurs and at 500-700 °C, Ni^{2+} is being reduced. Finally, 750-900 °C can be associated with the reduction of Mo^{4+} [27]. This is in accordance with the results in this project, although 800 °C do not seem to be high enough for complete reduction of Mo^{4+} because of the sudden drop in hydrogen consumption. In [28], they did a TPR test for a NiMo/Yzeolite catalyst and at 500 ° C octahedral Mo^{6+} is reduced to Mo^{4+} and at 730 ° C tetrahedral Mo^{6+} is reduced to Mo^{4+}. In Figure 2, the reduction taking place at 500 ° C could correspond to the reduction of the octahedral Mo^{6+}. Also, right before 730 ° C there is a small drop in hydrogen consumption, which increases again around 730 ° C. This might be the reduction of tetrahedral Mo^{6+}.

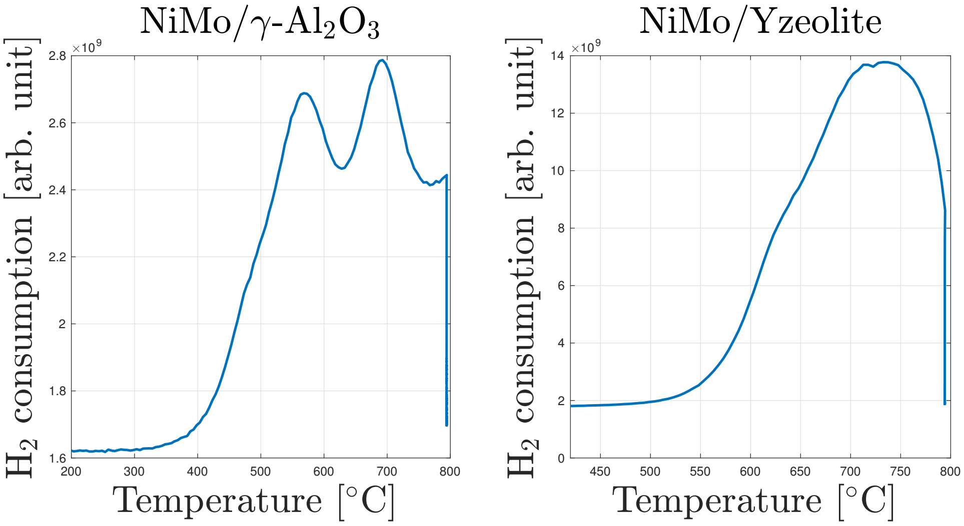

Figure 2: TPR profiles of NiMo/γ-Al_2O_3 and NiMo/Yzeolite with a pretreatment step. 2000ppm of hydrogen in Ar was used and the flow rate of hydrogen was 20 mL/min. The hydrogen and Ar were detected by a mass spectrometer.

The BET surface area, pore volume and pore size were submitted directly from the computer that records the data. The BET surface area was calculated in the linear region, before the hysteresis behavior starts, using Equation 3 and 4. The pore volumes reported for NiMo/γ-Al_2O_3, NiMo/Yzeolite and Mo/Yzeolite are single point adsorption total pore volume of pores less than 1200.135 Å width at P/Po=0.9836, 1253.728 Å width at P/Po=0.9843 and 1289.383 Å width at P/Po=0.9848 respectively. The pore sizes reported are the BJH Adsorption average pore width (4V/A) for all three catalysts. The results from BET are all presented in Table 1.

Table 1: Textural properties of the three calcined catalysts.

	BET surface area [m^2g^{-1}]	**Average Pore Volume [cm^3g^{-1}]**	**Average Pore Size [Å]**
NiMo/γ-Al$_2$O$_3$	155.0555	0.326732	74.279
NiMo/Yzeolite	412.9296	0.303114	53.097
Mo/Yzeolite	278.6790	0.312557	68.903

The results from XPS analyses of the calcined and reduced NiMo/γ-alumina catalysts, the calcined and reduced NiMo/Yzeolite catalysts and the reduced Mo/Yzeolite catalyst can be seen in Figure 3 and Figure 4. For the Mo3d spectra, the binding energies used are taken from [29] and the Ni2p spectra is compared with [30]. The calcined NiMo/γ-alumina and NiMo/Yzeolite catalysts are fully oxidized and as expected, the XPS results for these catalysts show no peaks at Mo metal (228 eV). In contrast, the results from the Mo3d spectra for the reduced catalysts show some signals for this binding energy, which could be an indication that some of the catalyst is in a metallic state. This is likely the case for NiMo/γ-alumina since the TPR result suggested that the catalyst have been reduced in the catalyst activation step. According to the XPS spectrum, however, it appears that the catalysts are not fully reduced because there are clear peaks at different molybdenum oxides for each reduced catalyst. But at the specific binding energies for molybdenum oxides, signals for the calcined catalysts are more distinct than for the corresponding reduced catalyst. This also leads to the suggestion that the catalyst has been at least partially reduced.

The Ni2p spectrum for the calcined and reduced catalysts, for both of the two support materials, have similar appearance and this might be because the nickel oxides have not been reduced in the same amount as the molybdenum oxides in the first place or due to the exposure to air. The exposure to air could have reoxidized both the metallic nickel and the metallic molybdenum. A study regarding oxidation of Mo containing catalyst has been conducted where the catalyst was examined by XPS. First, the fresh catalyst was analyzed and then it was exposed to air for three minutes followed by another analysis. The results showed an increase in the relative amount of both Mo (IV) oxide and Mo (VI) oxide at the surface of the catalyst [31]. For the XPS analyses in this thesis project, the three reduced samples were exposed to air to various extents. All three samples were put on the same sample holder in the following order: NiMo/γ-alumina, NiMo/Yzeolite and Mo/Yzeolite. Each pipetting took 1-2 minutes because several droplets had to be added to make sure the catalyst layer was fully covering the carbon rubber pad to exclude inaccurate carbon signals. After all of the catalysts were added, the samples were left for the ethanol to evaporate for another couple of minutes before putting it into the sample chamber. For all three reduced catalysts, however, it seems like some remained reduced during XPS analysis.

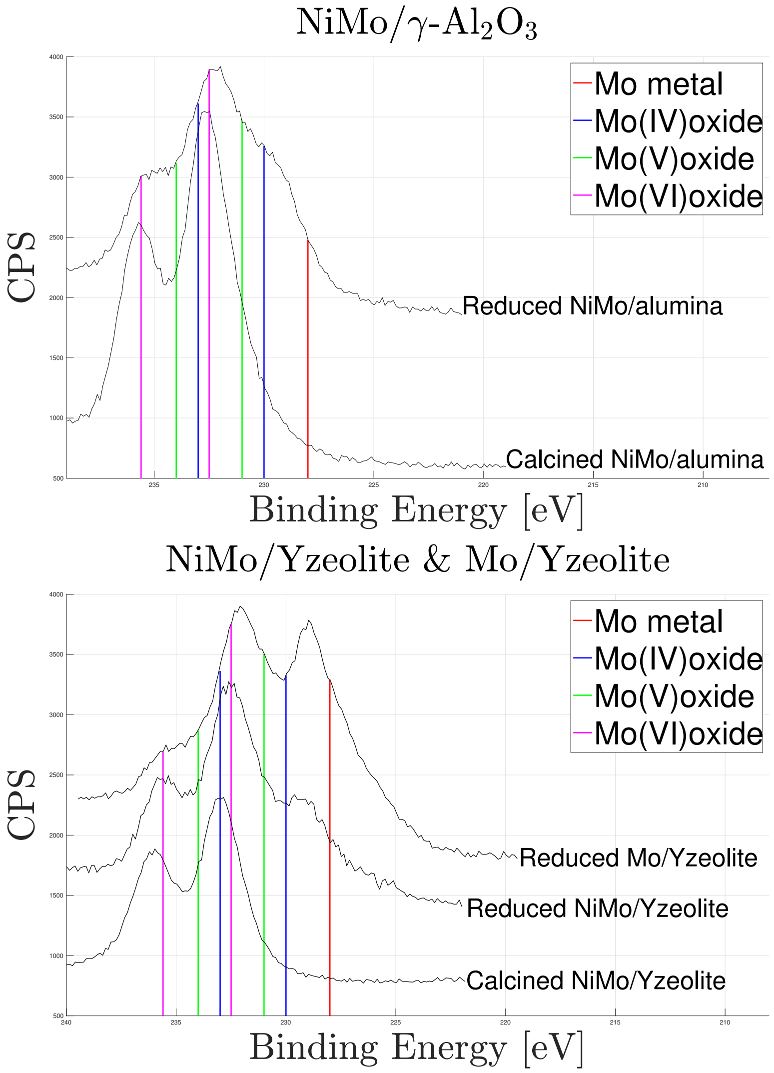

Figure 3: Mo3d spectra of the catalysts. a) Reduced and calcined NiMo/γ-Al$_2$O$_3$ catalysts. b) Reduced and calcined NiMo/Yzeolite and reduced Mo/Yzeolite catalysts.

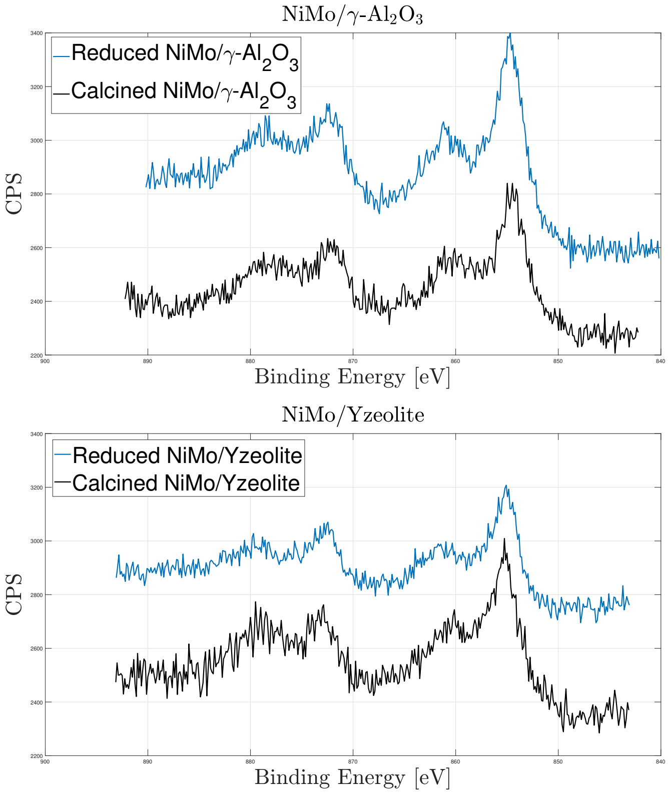

Figure 4: Ni2p spectra of the catalysts. The blue signals are from the reduced catalysts and the black signals are from the calcined catalysts. a) Reduced and calcined NiMo/γ-Al_2O_3 catalysts. b) Reduced and calcined NiMo/Yzeolite catalysts.

The TPR result for the NiMo/Yzeolite did not confirm that a temperature of 450 °C was enough for the reduction of it, but from the XPS results it is clear that it has been partly reduced. During the experiment, more hydrogen was available than in the TPR experiment and this seems to have led to reduction of molybdenum. Mo/Yzeolite has the most distinct shift to 228 eV and it could be due to it being placed on the sample holder last. Another possibility would be that there is no nickel that will compete for consumtion of hydrogen in the activation step. The placement of reduced catalysts on the sample holder could probably be done in a more effective way and this would probably give a greater peak area around 228 eV for all reduced catalysts. The peaks for Ni2p around 854 eV and 873 eV can be associated with Ni(II)oxide and the peak to the left of each of them is likely a satellite peak [30].

4.2. HDO Activity

Calibration curves for PPE, phenol and ethylbenzene along with all the coefficients used for GC analyses are presented in Appendix A. For the reduced catalysts, carbon balances are presented in Appendix B. Figure 5 shows one simple reaction mechanism of the model compound. All the different compounds that were detected have been grouped into either deoxygenated aromatics, oxygen-containing compounds or cycloalkanes. Which group the different compounds are included in can be seen in Appendix C. Mass balances for both reduced and sulfided catalysts are presented in Appendix D. Compounds detected at a mol% of 0.5 or less in the final sample (360 min) are not included in the mass balances, carbon balances and selectivity plots, but are reported in Appendix E. For the experiment with the NiMo/Yzeolite catalyst, the data from 35 and 300 min samples has been excluded because of poor carbon balances. One disappointing outcome regarding the catalytic activity tests was the carbon balances for NiMo/γ-alumina. Another experiment was conducted but there was a problem with the sampling line during the experiment. Because of the time limit, a third experiment was not conducted in this project. Even though the carbon balances in the first experiment with the NiMo/γ-alumina are poor, the results have been normalized and used for comparison with the other results. However, it should be emphasized that the experiments should be conducted again to verify the results.

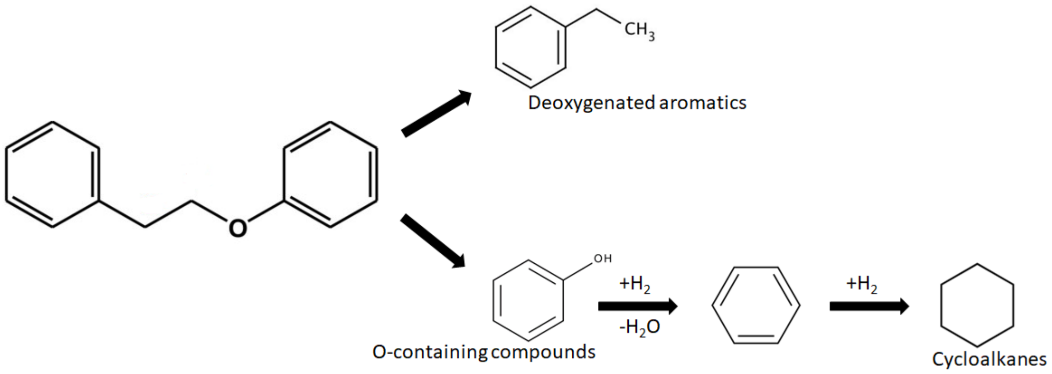

Figure 5: One possible reaction mechanism of the model compound PPE. First, one linkage in PPE is broken, which results in one deoxygenated aromatic, ethylbenzene, and one oxygen-containing compound, phenol. Second, the oxygen-containing compound is hydrodeoxygenated into benzene. At last, it is possible for benzene to be fully hydrogenated into cyclohexane, which is a cycloalkane.

Experimental results for sulfided NiMo catalysts were shared from the group. The results from the activity tests with reduced and sulfided catalysts are presented in Figure 6, Figure 7 and Figure 8. From the plots of conversion of PPE it is clear that all of the model compound in the feed has been consumed for all experiments. The two reduced catalysts with a zeolite support show slower conversion of PPE than the reduced NiMo/γ-alumina. Since the zeolite support is especially good for cracking, one possible explanation is that there is coke formation on the surface which would block some of the active sites. The pore sizes of both zeolite catalysts are smaller than for the alumina catalyst and the PPE conversion for the reduced catalysts follows the same order as pore size where the catalyst with the biggest pore size, NiMo/γ-alumina, has the fastest conversion of PPE. Thus, another possibility for the slower conversion for zeolite supported catalysts could be due to mass transfer limitations.

For NiMo/γ-alumina, it is clearly a difference between the selectivity of the reduced and the sulfided catalysts. The sulfided NiMo/γ-alumina catalyst have much higher HDO activity than the reduced catalyst and there are also several fully hydrogenated compounds for the sulfided catalyst. It is possible that the reduced catalysts could be reoxidized as a result of HDO, which would lead to a loss in activity. All three reduced catalysts are more selective towards oxygen-containing compounds compared to deoxygenated ones, while for the two sulfided catalysts the opposite can be observed. Among the reduced catalysts, NiMo/γ-alumina performed better with regard to HDO while both the reduced NiMo catalysts indicated a similar yield in deoxygenated compounds. The reduced catalysts performed differently according to HDO in the order of NiMo/γ-Al_2O_3, NiMo/Yzeolite and Mo/Yzeolite where the alumina catalyst gives the most deoxygenated compounds. This corresponds to the TPR results, which showed that the reduction of NiMo/γ-Al_2O_3 was easier to do than the reduction of the NiMo/Yzeolite catalyst. For the two sulfided catalysts, the NiMo/γ-Al_2O_3 also have the highest HDO activity. In Figure 8, the promoted and unpromoted reduced catalysts are compared and the HDO activity of the NiMo/Yzeolite is greater than that of Mo/Yzeolite. This could mean that nickel helps to increase the HDO activity of reduced NiMo catalysts as well as for the sulfided catalysts. Another possible explanation is that the NiMo catalyst is more easily reduced than the Mo catalyst. However, further investigation is needed to confirm this.

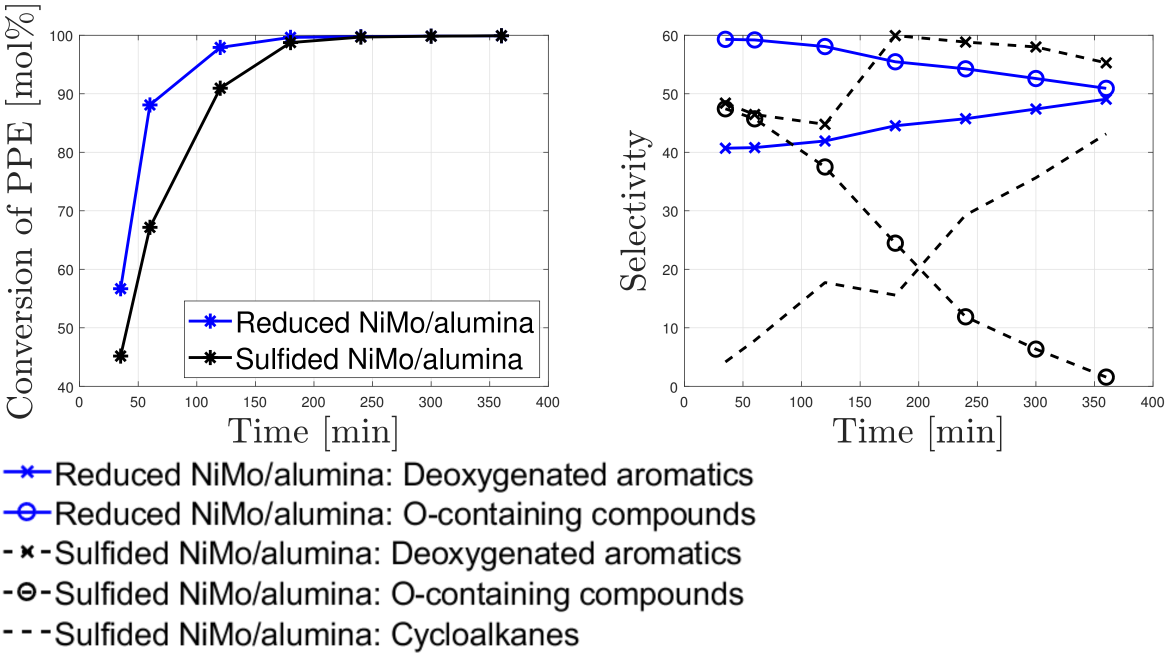

Figure 6: HDO activity for NiMo/γ-Al_2O_3. The reaction conditions were 320 °C, 50 bar hydrogen and a 1000 rpm stirring rate. a) Conversion of the model compound PPE. b) Selectivity plot.

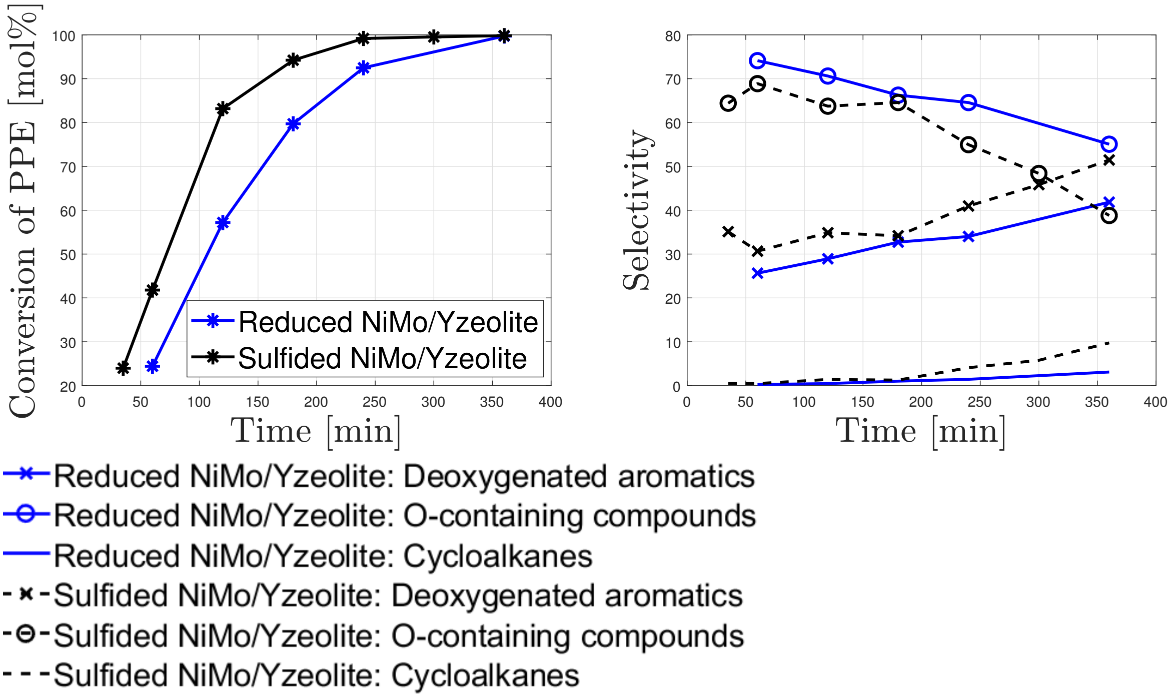

Figure 7: HDO activity for NiMo/Yzeolite. The reaction conditions were 320 °C, 50 bar hydrogen and a 1000 rpm stirring rate. a) Conversion of the model compound PPE. b) Selectivity plot.

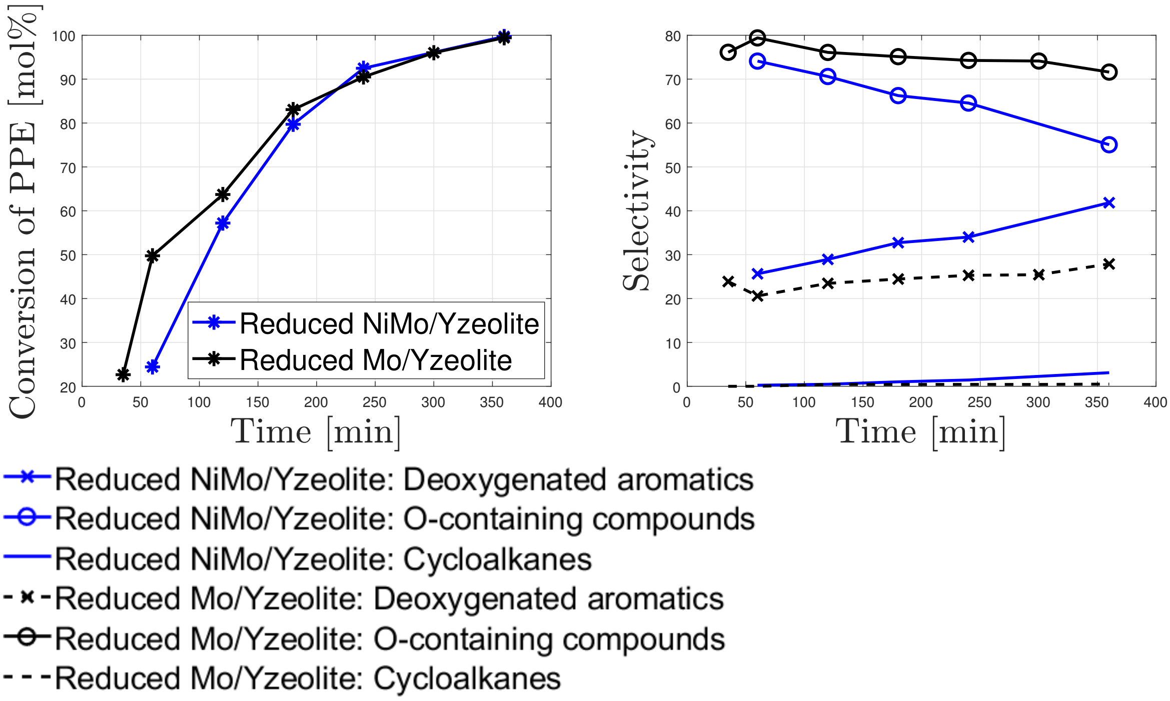

Figure 8: HDO activity for NiMo/Yzeolite and Mo/Yzeolite. The reaction conditions were 320 °C, 50 bar hydrogen and a 1000 rpm stirring rate. a) Conversion of the model compound PPE. b) Selectivity plot.

4.3. Future Work

The removal of oxygen in the reaction could probably reoxidize the catalyst and it would therefore be interesting to do an additional XPS of the catalyst after the activity experiment. Running experiments with calcined catalysts would give information if it was worth reducing the catalyst at a temperature of 450 °C.

In the experiment with sulfided catalysts, additional DMDS is added to keep the catalyst in a sulfided state. This could also be added in experiments with the reduced catalysts to study the selectivity during the exact same conditions. Also, sulfur impurities are often present in biomass and tests with a commonly corresponding amount could be used for studies to resemble real feedstock compositions.

5. Conclusion

The HDO activity for the sulfided catalysts was greater compared to the reduced ones. For the reduced catalysts, the HDO activity was in the following order: NiMo/γ-Al_2O_3, NiMo/Yzeolite and Mo/Yzeolite. The TPR results confirmed that the reactor temperature for reduction of NiMo/γ-Al_2O_3 was high enough, but the results did not verify that the NiMo/Yzeolite should be reduced. However, the XPS results show that all the catalysts had been partly reduced. The lower activity of the reduced catalysts may be due to the fact that they are not sufficiently reduced at 450 °C, which was the maximum possible temperature in this study.

References

[1] NE Nationalencyklopedin [Internet] Egnéus H, Svenningsson P; Bioenergi; [cited 2019-01-13]; [about 8 screens]. Available from: `http://www.ne.se/uppslagsverk/encyklopedi/lång/bioenerg`

[2] AccessScience [Internet]. West Lafayette: School of Agriculture and Biological Engineering; 2014. Biomass; [cited 2018-11-13]; [about 4 screens]. Available from: `https://doi.org/10.1036/1097-8542.083300`

[3] Schutyser W, Renders T, Van den Bosch S, Koelewijn SF, Beckham GT, Sels BF. Chemicals from lignin: An interplay of lignocellulose fractionation, depolymerisation, and upgrading. Chemical Society Review [Internet]. 2018 [cited 2018-16-11];47(3):852-908. Available from: `https://doi.org/10.1039/c7cs00566k`

[4] Pandey A, Bhaskar T, Stöcker M, Sukumaran RK. Recent Advances in Thermochemical Conversion of Biomass [Internet]. Knovel: Elsevier; 2015. Chapter 4, Catalysts for Thermochemical Conversion of Biomass. [cited 2018-11-14]. Available from: `https://app.knovel.com/hotlink/pdf/id:kt00UR3HC0/recent-advances-in-thermochemical/catalysts--introduction`

[5] Ojagh H. Hydrodeoxygenation (HDO) catalysts [dissertation]. Gothenburg: Chalmers University of Technology; 2018.

[6] A Dictionary of Chemical Engineering [Internet]. Oxford University Press: Schaschke C; 2014. Hydrotreating; [cited 2018-11-19]; [about 1 screen]. Available from: `http://www.oxfordreference.com/view/10.1093/acref/9780199651450.001.0001/acref-9780199651450-e-1483`

[7] Singh R, Prakash A, Balagurumurthy B, Bhaskar T. Recent Advances in Thermochemical Conversion of Biomass [Internet]. Knovel: Elsevier; 2015. Chapter 10, Hydrothermal Liquefaction of Biomass. [cited 2018-11-28]. Avialable from: `https://doi.org/10.1016/B978-0-444-63289-0.00010-7.`

[8] Aresta M; Dibenedetto A; Dumeignil F. Biorefinery - From Biomass to Chemicals and Fuels [Internet]. Knovel: De Gruyter; 2012. Chapter 8, Conversion of lignin: chemical technologies and biotechnologies – oxidative strategies in lignin upgrade. [cited 2018-11-28]. Available from: `https://app.knovel.com/hotlink/pdf/id:kt00U4FWV1/biorefinery-from-biomass/biorefiner-introduction`

[9] Gillet S, Aguedo M, Petitjean L, Morais ARC, de Costa Lopes AM, Łukasik RM, Anastas PT. Lignin transformations for high value applications: Towards targeted modifications using green chemistry. Green Chemistry [Inter-

net]. 2017 [cited 2018-11-20];19(18):4200-4233. Available from: https://doi.org/10.1039/c7gc01479a

[10] Prakash A, Singh R, Balagurumurthy B, Bhaskar T, Arora AK, Puri SK. Recent Advances in Thermochemical Conversion of Biomass [Internet]. Knovel: Elsevier; 2015. Chapter 16, Thermochemical Valorization of Lignin. [cited 2018-12-14]. Available from: https://app.knovel.com/hotlink/pdf/id:kt00UR3T6B/recent-advances-in-thermochemical/recent-adv-introduction-3

[11] Zhang C, Lu J, Zhang X, Macarthur K, Heggen M, Li H, Wang F. Cleavage of the lignin -O-4 ether bond: Via a dehydroxylation-hydrogenation strategy over a NiMo sulfide catalyst. Green Chemistry [Internet]. 2016 [cited 2018-11-21];18(24):6545-6555. Available from: https://doi.org/10.1039/c6gc01456a

[12] AccessScience [Internet]. Appleton: Chemical Sciences Division; 2014. Lignin; [cited 2018-11-13]; [about 3 screens]. Available from: https://doi.org/10.1036/1097-8542.382150

[13] Sasol [Internet]. [cited 2019-02-11]. Available from: https://www.sasolgermany.de/index.php?id=dispersible_aluminas0

[14] Arora P, Ojagh H, Woo J, Lind Grennfelt E, Olsson L, Creaser D. Investigating the effect of Fe as a poison for catalytic HDO over sulfided NiMo alumina catalysts. Applied Catalysis B: Environmental [Internet]. 2018-07-05 [cited 2019-01-05];227:240-251. Available from: https://doi.org/10.1016/j.apcatb.2018.01.027

[15] Zeolyst International [Internet]. [cited 2019-02-11]. Available from: https://www.zeolyst.com/our-products/standard-zeolite-powders/zeolite-y.html

[16] AccessScience [Internet]. Evanston, New Haven: Yale University, Northwestern University; 2017. Catalysts; [cited 2018-11-20]; [about 5 screens]. Available from: https://doi.org/10.1036/1097-8542.113200

[17] Chiusoli, Gian Paolo Maitlis, Peter M. Metal-Catalysis in Industrial Organic Processes [Internet]. Knovel: Royal Society of Chemistry; 2006. Appendix 2: Some Basic Aspects of Surface Science Related to Heterogeneously Catalyzed Reactions A2.1 Background. [cited 2019-01-13]. Available from https://app.knovel.com/hotlink/pdf/id:kt007MFP35/metal-catalysis-in-industrial/background

[18] Červený, L. Catalytic Hydrogenation [Internet]. Knovel: Elsevier; 1986. Chapter 18: Selective Hydrogenation Applied to the Refining of Petrochemical Raw Materials Produced by Steam Cracking. vail-

able from: https://app.knovel.com/hotlink/pdf/id:kt00TXFA05/catalytic-hydrogenation/catalytic--introduction-4

[19] Ding S, Li Z, Li F, Wang Z, Li J, Zhao T, Lin H, Chen C. Catalytic hydrogenation of stearic acid over reduced NiMo catalysts: Structure–activity relationship and effect of the hydrogen-donor. Applied Catalysis A [Internet]. 2018 [cited 2018-16-11];566:146-154. Available from: https://doi.org/10.1016/j.apcata.2018.08.028

[20] Basrur A, Sabde D. Industrial Catalytic Processes for Fine and Specialty Chemicals [Internet]. Knovel: 2016. Chapter 4: Catalyst Synthesis and Characterization. [cited 2019-01-17]. Available from: http://app.knovel.com/web/view/pdf/show.v/rcid:kpICPFSC03/cid:kt01101ZP3/viewerType:pdf//root_slug:industrial-catalytic/url_slug:catalyst-synthesis-characterization?cid=kt01101ZP3&q=Catalyst%20Synthesis%20and%20Characterization&b-q=Catalyst%20Synthesis%20and%20Characterization&sort_on=default&b-subscription=true&b-group-by=true&page=1&b-sort-on=default&b-content-type=all_references&include_synonyms=yes

[21] Julbe A, Drobek M (2016) Zeolite Y Type. In: Drioli E., Giorno L. (eds) Encyclopedia of Membranes. Springer, Berlin, Heidelberg . [cited 2019-01-05]. Available from https://doi.org/10.1007/978-3-662-44324-8_608

[22] Harris DC. Quantitative Chemical Analysis. 9th ed. New York: W. H. Freeman and Company; 2016.

[23] Gervasini A. (2013) Temperature Programmed Reduction/Oxidation (TPR/TPO) Methods. In: Auroux A. (eds) Calorimetry and Thermal Methods in Catalysis. Springer Series in Materials Science, vol 154. Springer, Berlin, Heidelberg. [cited 2018-12-05].

[24] Murzin, Dmitry Yu. (2013). Engineering Catalysis - 2.1 Catalyst Design. De Gruyter. [cited 2018-12-03]. Available from: https://app.knovel.com/hotlink/pdf/id:kt00TXC2NI/engineering-catalysis/catalyst-design

[25] Samal, Prasan K. Newkirk, Joseph W.. (2015). ASM Handbook, Volume 7 - Powder Metallurgy (2015) - 14. Surface Area, Density, and Porosity of Powders. ASM International. [cited 2018-12-18]. Available from: https://app.knovel.com/hotlink/pdf/id:kt010RU272/asm-handbook-volume-7/surface-area-density

[26] Ramachandran, V.S. Beaudoin, James J.. (2001). Handbook of Analytical Techniques in Concrete Science and Technology - 14.1 Introduction. William Andrew Publishing/Noyes. [cited 2018-12-05]. Avail-

able from: https://app.knovel.com/hotlink/pdf/id:kt0052L5Y5/handbook-analytical-techniques/pore-structure-introduction

[27] Yi X, Guo D, Li P et al. One pot synthesis of NiMo-Al2O3catalysts by solvent-free solid-state method for hydrodesulfurization. RSC Advances [Internet]. 2017-11-24 [cited 2019-01-05];7(86):54468-54474. Available from: https://doi.org/10.1039/c7ra11892a

[28] Zhang Z, Wang Q, Chen H, Zhang X. Hydroconversion of Waste Cooking Oil into Green Biofuel over Hierarchical USY-Supported NiMo Catalyst: A Comparative Study of Desilication and Dealumination. Catalysts [Internet]. 2017-09-22 [cited 2019-01-15];7(10)281. Available from https://doi.org/10.3390/catal7100281

[29] Baltrusaitis J, Mendoza-Sanchez B, Fernandez V et al. Generalized molybdenum oxide surface chemical state XPS determination via informed amorphous sample model. Applied Surface Science [Internet]. 2015-01-30 [cited 2019-01-18];326:151-161. Available from: https://doi.org/10.1016/j.apsusc.2014.11.077

[30] Thermo Scientific XPS simplified [Internet]. [cited 2018-12-27]. Available from: https://xpssimplified.com/elements/nickel.php

[31] Baily C, Mack P, Scientific T. Investigating the Oxidation of a Cobalt-based Catalyst Using X-ray Photoelectron Spectroscopy. Application Note 52373. 2012. Thermo Fisher Scientific Inc. [cited 2019-01-05].

A. Appendix

Calibration curves and coefficients

Calibration curves of 2-phenethyl phenyl ether (PPE), phenol and ethylbenzene can be seen in Figure 9. The coefficient for each compound was determined by linear regression through origin and for the remaining compounds, coefficients were already determined by the team. For some compounds detected, external calibration curves had not been conducted. For these compounds, a calibration coeffient for a compound with the same amount of carbon, or the nearest amount and most similar structure, was used. The coefficients determined in the calibration curves are specified in Table 2 along with all coefficients that has been used for quantification of specific compounds. The solutions used for the calibration curves are in the concentration of 0<mol%<5 in dodecane, which is based on the concentration of PPE in the feed.

Table 2: The calibration coefficients for quantification of the detected compounds.

Compound	**Coefficient**
PPE	4.1086e+08
Phenol	1.4181e+08
Ethylbenzene	1.9864e+08
Cyclohexane	1.4368e+08
Toluene	1.8806e+08
Benzyl Phenol	4.0052e+08
Benzyl Phenyl Ether	3.5313e+08

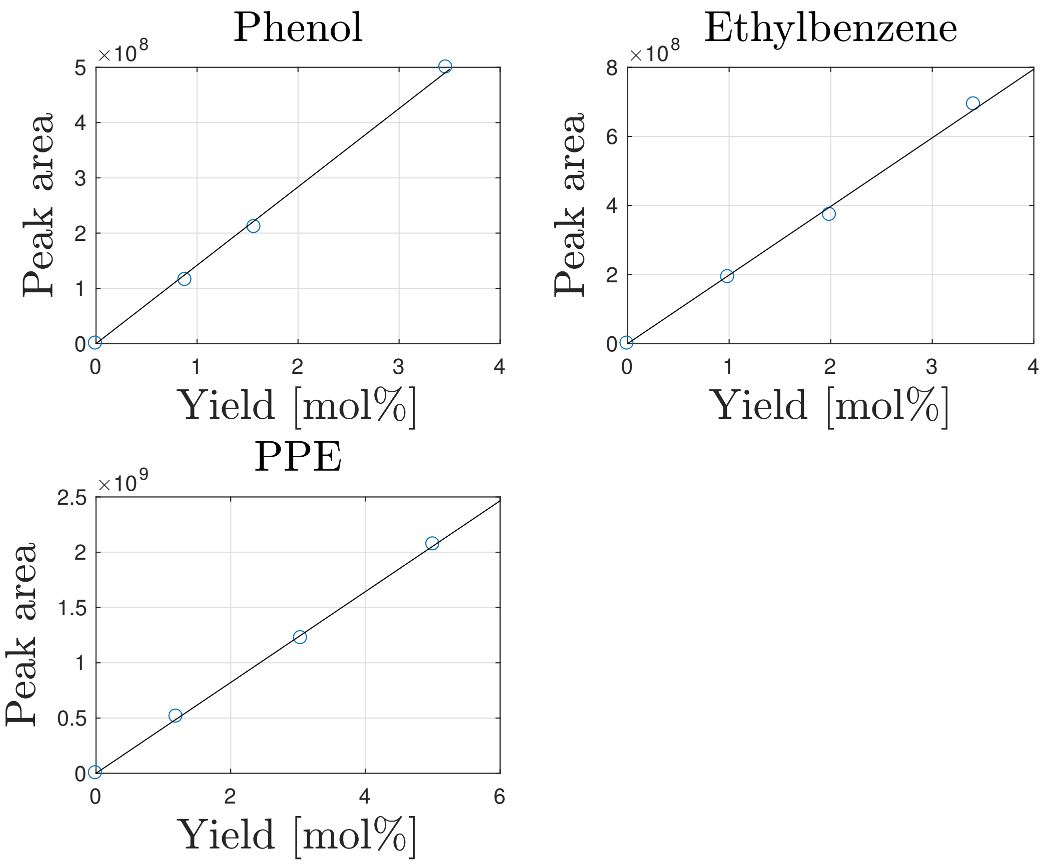

Figure 9: Calibration curves for phenol, ethylbenzene and PPE.

B. Appendix

Carbon Balances

For the experiments with NiMo/γ-alumina, NiMo/Yzeolite and Mo/Yzeolite, 5.7993 g, 5.7483 g and 5.7966 g of PPE was used respectively.

Table 3: Carbon balances where the amount of carbon for each sampling time was compared to the amount of carbon of the model compound, PPE, in the feed. A value >1.0 indicates that the amount of carbon in the sample exceeds the amount of carbon in the feed. A value <1.0 indicates that the amount of carbon in the sample is below the amount the carbon in the feed.

	35 min sample	60 min sample	120 min sample	180 min sample	240 min sample	300 min sample	360 min sample
NiMo/-alumina	1.06	1.07	1.12	1.18	1.15	1.16	1.19
NiMo/Y zeolite	1.35	0.90	0.84	0.91	0.96	1.30	0.89
Mo/Y zeolite	0.90	0.85	1.05	0.92	0.94	0.93	1.00

C. Appendix

Deoxygenated aromatics, O-containing compounds and Cycloalkanes

Table 4: The compounds detected for both the reduced and sulfided catalysts and which type of compound they are.

Compound	**Type of compound**
Methyl-cyclopentane	Cycloalkane
Cyclohexane	Cycloalkane
Ethylcyclohexane	Cycloalkane
Benzene	Deoxygenated aromatic
Ethylbenzene	Deoxygenated aromatic
Toluene	Deoxygenated aromatic
Phenethyl Cyclohexane	Deoxygenated aromatic
Benzene, diethyl-	Deoxygenated aromatic
Bibenzyl	Deoxygenated aromatic
Methyl Phenol	O-containing compound
Phenol	O-containing compound
Phenol, ethyl-	O-containing compound
Phenol, cyclohexyl-	O-containing compound
Phenethylphenol	O-containing compound
Benzyl phenol	O-containing compound
Methanone, bis(3-methylphenyl)-	O-containing compound
2-(4-Benzylphenyl)propan-2-ol	O-containing compound

D. Appendix

Mass balances

Mass balances (mol%) from the experiments with the three reduced catalysts are presented in Table 10, Table 6 and Table 7. Also, the coefficient that was used for quantification is reported. The mass balances for sulfided catalysts are presented in Table 8 and Table 9.

Table 5: Mass balances for NiMo/γ-Al_2O_3.

	35 min sample	60 min sample	120 min sample	180 min sample	240 min sample	300 min sample	360 min sample	Coefficient
Benzene	0.35	0.62	1.31	3.96	4.85	6.24	7.70	Cyclohexane
Ethylbenzene	33.26	46.99	54.23	58.66	57.25	58.80	60.18	Ethylbenzene
Phenol	32.73	44.70	50.17	51.71	48.01	47.54	46.73	Phenol
Bibenzyl	0.09	0.21	0.40	0.72	0.95	1.15	1.40	PPE
Phenol, 2-cyclohexyl-	0.12	0.31	0.52	0.78	0.88	0.96	1.02	Benzyl Phenol
Phenol, 4-cyclohexyl	0.00	0.06	0.19	0.41	0.57	0.74	0.8	Benzyl Phenol
2-phenethyl phenyl ether (PPE)	43.32	11.91	2.08	0.36	0.24	0.14	0.09	PPE
Phenethylphenol	13.17	19.74	21.57	21.03	20.47	19.59	18.76	PPE
2-(4-Benzylphenyl)propan-2-ol	3.09	4.58	5.02	4.97	4.87	4.64	4.49	PPE

Table 6: Mass balances for NiMo/Yzeolite.

	35 min sample	60 min sample	120 min sample	180 min sample	240 min sample	300 min sample	360 min sample	Coefficient
Methyl Cyclopentane	0	0.07	0.26	0.89	1.52	5.16	3.18	Cyclohexane
Benzene	2.18	0.68	1.78	4.49	6.24	16.76	9.05	Cyclohexane
Ethylbenzene	5.77	5.69	12.56	21.30	26.38	41.67	29.24	Ethylbenzene
Toluene	0.27	0.21	0.45	0.90	1.09	2.16	1.33	Toluene
Phenol	10.79	8.85	19.37	31.82	38.22	53.56	33.06	Phenol
Benzene, 1,2-diethyl-	0.11	0.14	0.33	0.50	0.61	0.73	0.77	Ethylbenzene
Phenol, 2-ethyl-	0.13	0.23	0.53	0.81	1.01	1.21	1.40	Ethylbenzene
Bibenzyl	0	0.51	0.94	1.32	1.64	1.85	2.51	PPE
2-phenethyl phenyl ether (PPE)	119.96	75.58	42.80	20.29	7.52	1.86	0.28	PPE
Phenethylphenols	8.74	11.82	18.95	24.55	28.32	26.4	20.79	PPE
Methanone, bis(3-methylphenyl)-	0	0	0.35	0.53	0.70	0.81	1.20	PPE

Table 7: Mass balances for Mo/Yzeolite.

	35 min sample	60 min sample	120 min sample	180 min sample	240 min sample	300 min sample	360 min sample	Coefficient
Methyl-cyclopentane	0	0	0.36	0.36	0.42	0.43	0.55	Cyclohexane
Benzene	0.58	0.84	2.18	2.34	2.87	3.04	4.13	Cyclohexane
Ethylbenzene	3.78	7.57	15.41	17.05	19.59	20.60	24.17	Ethylbenzene
Toluene	1.39	0.65	0.93	0.82	0.90	0.95	1.10	Toluene
Phenol	8.68	14.92	28.21	29.00	32.08	32.42	36.41	Phenol
Phenol, 2-ethyl-	0	0	0.24	0.41	0.50	0.58	0.54	Ethylbenzene
Bibenzyl	0.15	0.33	0.55	0.67	0.75	0.87	1.08	PPE
2-phenethyl phenyl ether (PPE)	77.35	50.25	36.29	16.94	9.50	3.98	0.57	PPE
2-(4-Benzylphenyl)propan-2-ol	0.49	1.01	1.59	1.67	1.73	1.87	1.90	PPE
Phenethylphenol	9.64	20.27	31.81	33.08	36.50	39.33	39.42	PPE

Table 8: Mass balances for Sulfided NiMo/γ-Al_2O_3.

	35 min sample	60 min sample	120 min sample	180 min sample	240 min sample	300 min sample	360 min sample
Cyclohexane	2.19	6.24	16.86	13.65	30.63	36.88	43.12
Ethylcyclohexane	0.04	0.13	0.53	0.77	1.46	2.12	2.97
Toluene/Ethylbenzene	25.64	37.05	41.44	51.56	59.29	57.53	52.55
Phenol	20.84	30.63	29.39	16.71	9.87	5.49	1.39
Phenethyl Cyclohexane	0.28	0.77	2.48	3.88	5.20	5.93	6.51
2-phenethyl phenyl ether (PPE)	54.83	32.83	9.05	1.25	0.31	0.16	0.08
Total benzyl phenol	4.56	6.59	7.38	5.92	3.15	1.46	0.29

Table 9: Mass balances for Sulfided NiMo/Yzeolite.

	35 min sample	60 min sample	120 min sample	180 min sample	240 min sample	300 min sample	360 min sample
Methyl Cyclopentane	0.12	0.19	1.32	1.16	4.40	5.53	9.95
Benzene/Cyclohexane	1.03	1.08	3.88	2.87	7.75	8.52	13.70
Ethylbenzene	7.16	10.47	27.00	26.33	32.97	30.63	33.71
Toluene	0.23	0.24	0.63	0.56	0.95	1.37	1.32
Phenol	8.35	15.76	37.88	35.20	40.08	32.70	31.03
Methyl Phenol	0.32	0.62	1.53	1.72	2.36	3.34	3.98
Bibenzyl	0.32	0.54	1.30	1.61	2.44	3.35	3.83
2-phenethyl phenyl ether (PPE)	76.02	58.21	16.83	5.79	0.83	0.48	0.18
Total Phenethylphenol	7.36	11.32	20.56	22.35	16.73	10.27	4.62

E. Appendix

Minor findings

Table 10: Compounds detected in an amount of 0.5 mol% or less. x indicates that the compound has been detected for the specific catalyst. Also, the different coefficients used for quantification are presented.

Compound	**NiMo/γ-alumina**	**NiMo/Yzeolite**	**Mo/Yzeolite**	**Coefficient**
Cyclohexane, methyl-		x		Toluene
Benzene, propenyl-		x		Ethylbenzene
Phenol, methyl-	x	x		Benzyl Phenol
Phenol, ethyl-	x			Ethylbenzene
Benzene, cyclohexyl-	x			Benzyl Phenol
Diphenyl ether	x	x		Benzyl Phenyl Ether
Benzene, 1,1'-ethylidenebis-	x			PPE
2-Benzylidenecyclohexanol		x		Benzyl Phenyl Ether
Benzene, (2-cyclohexylethyl)-	x			PPE
2-Cyclohexen-1-one, 3-phenyl		x		Benzyl Phenyl Ether
Benzene, 1,1'-(1-methyl-1,3-propanediyl)bis-	x		x	PPE
Benzene, 1,1'-(1-methyl-1,2-ethanediyl)bis-		x		PPE
4-Methyl-2-(phenylacetyl)phenol		x	x	PPE
2-Methyl-6-(1-methyl-1-phenylethyl)phenol			x	PPE
2-(4-Benzylphenyl)propan-2-ol		x		PPE